Inorganic Chemistry Communications 126 (2021) 108467

Contents lists available at ScienceDirect

Inorganic Chemistry Communications

journal homepage: www.elsevier.com/locate/inoche

Short communication

Exploring boron distributions in MFI-type borosilicates

Xiaona Liu [a,b], Nana Yan [a], Chao Ma [a,c], Lei Wang [d], Peng Tian [a], Peng Guo [a,*], Zhongmin Liu [a,b]

[a] National Engineering Laboratory for Methanol to Olefins, Dalian National Laboratory for Clean Energy, Dalian Institute of Chemical Physics, Chinese Academy of Sciences, Dalian 116023, China
[b] University of Chinese Academy of Sciences, Beijing 100049, China
[c] Zhang Dayu School of Chemistry, Dalian University of Technology, Dalian 116024, China
[d] School of Chemistry and Molecular Engineering, Nanjing Tech University, Nanjing 211800, China

ARTICLE INFO

Keywords:
Zeolite
Borosilicates
Distribution of boron
Rietveld Refinement
Host–guest interaction

ABSTRACT

In this study, we have synthesized four **MFI**-type borosilicate zeolites with different B/Si ratios using tetrapropylammonium (TPA^+). The preferred location of boron atoms and structural roles of TPA^+ were investigated by Rietveld refinement. It revealed that boron-rich position T9 locates in the four-ring of *mel* composition building unit (CBU) and T5 locates in the five-rings of *mfi* CBU. Inspired by the structural roles of TPA^+ in this series of BMFI-TPA samples, we successfully replaced TPA^+ by Na^+ and commercialized linear organic molecules for synthesizing **MFI**-type borosilicates. Using this strategy, another five BMFI samples were obtained. Two of them are well-crystallized without any impurity, which enables us to further investigate the structural information. The results show that boron-rich positions were also in the four- and five-rings. Moreover, the locations of structural-directing agents were consistent with what we expected. The preferred locations of boron atoms unravelled here may provide a new way of tailoring locations of Brønsted acids.

Conventional zeolites are microporous crystalline aluminosilicates with orderly distributed channels or/and cavities of the molecular size. The basic building unit tetrahedron TO_4 (T = Si or Al) is further linked with the adjacent one, generating a three-dimensional (3D) framework. Unit now, there have been 253 framework type codes (FTCs) approved by International Zeolite Association-Structure Committee (IZA-SC) [1,2]. When Si atoms within the framework are replaced by Al, the zeolite framework will possess the negative charge, which can be balanced by the inorganic cations, organic cations, or both, called structural directing agents (SDAs). Nowadays, a variety of hetero-atoms have been introduced in the zeolite framework, such as B, P, Ti, V, Mn, Fe, Co, Ni, Zn, Ga, Ge, etc. Such chemical extensions not only enrich the structural diversities, but also alter the catalytic performance significantly. Among these zeolites with exotic hetero-atoms, the borosilicate zeolites have been paid increasing attention since 1) the protonated borosilicate zeolites have the unique weak Brønsted acids [3]; 2) boron atoms are preferred to distribute orderly and simultaneously locate in the specific building unit, which is distinct from the aluminum distribution in the conventional aluminosilicate zeolite [4–10]; 3) the further precise control of stronger Brønsted acid sites (Al-OH-Si) can be realized through the aluminum reinsertion into the borosilicate zeolites after the deboronation process, especially for the 10 × 12-ring borosilicate zeolites [11,12].

Being insightful to the aforementioned unique merits of borosilicate zeolites, it is closely associated with the distribution of boron in the zeolite framework. Although such spectral characterizations as IR [13,14] and NMR [14] can confirm the presence of four-coordinated boron within the zeolite framework, it is challenging to determine the atomic coordinate of boron within one unit cell. The convectional single-crystal X-ray diffraction (SCXRD) technique can probe the crystallographic structure in real space through analyzing the 3D X-ray diffraction and then phasing the reflections in reciprocal space. However, this approach is limited by the crystal size. Normally, a crystal larger than twenty micrometers is required for the in-house single-crystal X-ray diffractometer. In this case, powder X-ray diffraction (PXRD) becomes an alternative approach for the structural elucidation of nanocrystals. It can be used for determining the novel and complicated zeolite structures. For example, a small pore zeolite EU-12 (FTC: **ETL**)[15] with the two-dimension (2D) channel system was solved from PXRD using direct method. The novel structures of other zeolites, such as IM-20 (**UWY**) [16], ITQ-52 (**IFW**)[17], Uio-6 (**OSI**)[18], ERS-7 (**ESV**)[19] and SSZ-82 (**SEW**) [7] were also determined using PXRD data solely. Moreover, PXRD can also explore locations of organic structure-directing agents (OSDAs) and the interaction between OSDAs and framework through

* Corresponding author.
E-mail address: pguo@dicp.ac.cn (P. Guo).

https://doi.org/10.1016/j.inoche.2021.108467
Received 22 December 2020; Received in revised form 10 January 2021; Accepted 11 January 2021
Available online 15 January 2021

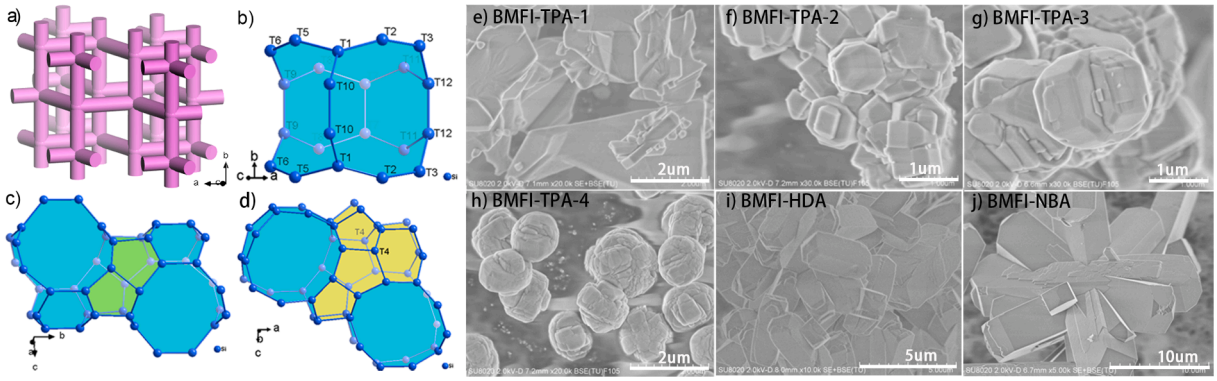

Fig. 1. (a) channel system of **MFI** framework. The overall channel system can be categorized into three regions (b) region I marked in blue is the cross channel, (c) Region II highlighted in green is the place between two cross channels (in blue) along the *b*-axis, and (d) Region III highlighted in yellow is the location between two cross channels (in blue) along the *a*-axis. SEM images of six as-made samples (e) BMFI-TPA-1, (f) BMFI-TPA-2, (g) BMFI-TPA-3, (h) BMFI-TPA-4, (i) BMFI-HDA, (j) BMFI-NBA. (For interpretation of the references to colour in this figure legend, the reader is referred to the web version of this article.)

Table 1
Unit cell compositions of the six samples.

Sample	Unit cell composition
BMFI-TPA-1	$\|(TPA^+)_{4.41}(H_2O)_{1.79}(OH^-)_{3.16}\|[Si_{94.75}B_{1.25}O_{192}]$
BMFI-TPA-2	$\|(TPA^+)_{4.36}(H_2O)_{3.10}(OH^-)_{2.23}\|[Si_{93.87}B_{2.13}O_{192}]$
BMFI-TPA-3	$\|(TPA^+)_{4.3}(H_2O)_{4.55}(OH^-)_{1.12}\|[Si_{92.82}B_{3.18}O_{192}]$
BMFI-TPA-4	$\|(TPA^+)_{3.93}(H_2O)_{4.87}(H^+)_{0.28}\|[Si_{91.79}B_{4.21}O_{192}]$
BMFI-HDA	$\|(HDA)_{8.07}(H_2O)_{0.74}(Na^+)_{1.04}(H^+)_{2.78}\|[Si_{92.18}B_{3.82}O_{192}]$
BMFI-NBA	$\|(NBA)_{7.58}(H_2O)_{3.684}(Na^+)_{0.24}(H^+)_{3.9}\|[Si_{91.86}B_{4.14}O_{192}]$

Rietveld refinement combined with the simulated annealing algorithm. For instance, our group recently has probed the host–guest interaction in the as-made SAPO-34/44 (**CHA**)[20], as-made and probe-molecule-adsorbed ferrierites (**FER**) [21]. Using this combined methodology, the rich aluminum T site has been identified as T1 in the aluminosilicate ferrierite synthesized by Na^+ and pyridine as SDAs. Smeets and co-workers investigated the locations of OSDAs in six borosilicate zeolites templated by complicated and expensive OSDAs by Rietveld refinement and then compared OSDAs' locations determined by the molecular modeling [22]. However, their structures are synthesized by complex and expensive OSDAs, which hinders further investigations regarding the fine regulation of boron contents and their distribution trend.

In this study, we select the well-known **MFI**-type borosilicate zeolite (denoted as BMFI) as the structural model since they can be conveniently synthesized by commercialized tetrapropylammonium (TPA^+), and their B/Si ratios can be tunable. Therefore, the preferred location of boron atoms with changing the B/Si ratio has been investigated systemically through Rietveld refinement. Furthermore, inspired by the structural roles of TPA^+ unraveled from the Rietveld refinement result, inorganic cations combined with the linear organic molecules are proposed as efficient SDAs to synthesize **MFI**-type borosilicates.

Typical synthetic procedures of BMFI samples were as follows: fumed silica was added to an aqueous solution containing H_3BO_3, NaOH, and OSDA under stirring. Some calcined silicalite-1 seeds synthesized by a previously reported procedure [9] were added and stirred for another hour. Finally, the mixture was transferred to a stainless-steel autoclave and crystallized. The detailed synthesis conditions are listed in Table S1.

The idealized **MFI** framework has 12 T atoms in the asymmetric unit with the space group *Pnma* (No. 62). It has straight 10-ring channels along the *b*-axis and zig-zag 10-ring channels along the *a*-axis, respectively. These two channels interconnect at the so-called cross channels. In this case, the overall channel system can be categorized into three regions (Fig. 1a–d). From the structural descriptions above, it is unambiguous that cross channels (Region I) dominate the overall channel system and most of T atoms locate around the cross channels. Now there is a scientific curiosity regarding the distribution of boron within the

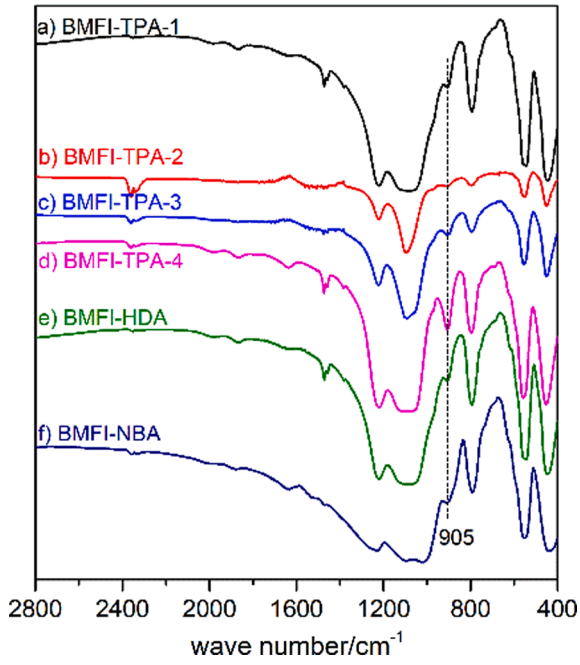

Fig. 2. FT-IR spectra of (a) BMFI-TPA-1, (b) BMFI-TPA-2, (c) BMFI-TPA-3, (d) BMFI-TPA-4, (e) BMFI-HDA, and (f) BMFI-NBA.

MFI framework. Therefore, a series of **MFI**-type borosilicates with different boron contents have been synthesized by the conventional hydrothermal synthesis, denoted as BMFI-TPA-1, BMFI-TPA-2, BMFI-TPA-3, and BMFI-TPA-4, respectively. Both the PXRD patterns (Figure S1) and SEM images (Fig. 1e–j) confirm that these samples are highly crystalline pure phases. The content of Si and B are obtained from ICP results. The number of H_2O and TPA^+ in the unit cell are deduced by TG measurements (Figure S2). The summarized unit cell compositions are listed in Table 1. It is worth noting that the number of boron within one unit cell can be tuned from 1 to 4 approximately. Fig. 2 shows the FT-IR spectra in the 400–2800 cm^{-1} region of these four as-made samples. The peaks at around 905 cm^{-1} are due to the symmetry stretching vibration of tetracoordinated boron in the framework [13]. However, the locations of boron within the **MFI** framework remains elusive through such characterizations. Thus, the samples were further investigated by Rietveld refinement combined with the simulated annealing algorithm.

The initial structural model of the **MFI** framework was adopted from

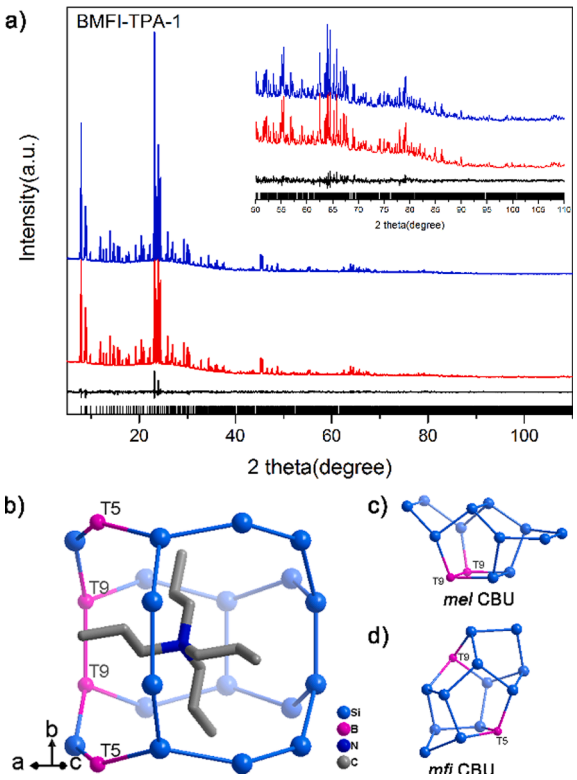

Fig. 3. (a) Final Rietveld refinement plots of BMFI-TPA-1. The observed, calculated, and difference curves are in blue, red, and black, respectively. The vertical bars indicate the positions of Bragg peaks (Cu Ka1, λ = 1.5406 Å). The inset is the high-angle part of the profiles. (b) The location of TPA^+ in the cross channel of BMFI-TPA-1 and boron-rich positions. (c) T9 is in the four-ring of *mel* CBU, and (d) T5 locates in the five-ring of *mfi* CBU in the BMFI-TPA-1. (For interpretation of the references to colour in this figure legend, the reader is referred to the web version of this article.)

IZA-database. Appropriate scale factor could be obtained between observed and calculated data from 60 to 110° in 2θ. Applying this scale factor to the whole pattern, the difference map could be obtained. Then, simulated annealing algorithms were employed to determine the locations and orientations of TPA^+. The detailed procedures of Rietveld refinement and final results are displayed in SI (Table S2, Fig. 3, and Figures S3 – S6). The results show that boron-rich T sites are distributed at T5 and T9 positions. The occupancies of boron on the T5 and T9 positions are 8% and 7.6% for BMFI-TPA-1, 15.6% and 11.0% for BMFI-TPA-2, 12.0% and 7.9% for BMFI-TPA-3, 30.2% and 22.4% for BMFI-TPA-4, respectively. It is clear to see that the unit cell shrinks with the increasing incorporation of boron (Table S2). It is worth noting that the boron-rich position T9 is in the four-rings of the *mel* CBU (Fig. 3c). This phenomenon has also been observed in other borosilicates, such as EMM-26 (**EWS**)[4], MCM-70 (**MVY**)[5], SSZ-87 (**IFW**)[6], and SSZ-82 (**SEW**)[7] (as shown in Figure S7). T5 locates in the five-rings of *mfi* CBUs (Fig. 3d).

Rietveld refinement reveals that there is one TPA^+ in each cross channel, which is consistent with the result from TG (Figure S2). It also shows that two propyl groups of TPA^+ point towards the straight 10-ring channels along the *b*-axis, while the rest extend to the zig-zag 10-ring channels along the *a*-axis (Fig. 3b). Inspired by the structural role of TPA^+ revealed by Rietveld refinement, we tentatively replace the classical OSDA TPA^+ by commercialized linear organic molecules (occupy Region I and II) (Figure S8a) and the inorganic cations (support the 10-ring pore opening along the *a*-axis) (Figure S8b) or organic molecules (stabilize Region III) (Figure S8c) for synthesizing **MFI**-type borosilicates. Therefore, we designed the following experiments.

Inorganic cations Na^+ and several linear organic molecules such as 1,6-hexamethylenediamine (HDA), n-butylamine (NBA), 1-ethylimidazole (EID), n-butanol (NBO), and 1,6-hexanediol (HDO) were selected for synthesizing the **MFI**-type borosilicates tentatively. The PXRD patterns (Figure S1 and S9) and SEM images (Fig. 1 and S10) demonstrate that the main products are **MFI**-type borosilicates, which has well proven our hypothesis. In order to identify the locations of OSDAs and inorganic cations at the atomic level, Rietveld refinement combined with the simulated annealing algorithm is utilized as well. Since such structural characterization technique has a strict requirement of the sample quality, many endeavors have been devoted to synthesizing well-crystallized **MFI**-type borosilicates without any undesirable impurity. In this case, BMFI-HDA and BMFI-NBA samples satisfying with Rietveld refinement requirements are chosen for further structural investigations. ICP measurements (Table 1) and IR spectra (Fig. 2) confirm that boron has been incorporated into the framework of BMFI-HDA and BMFI-NBA, showing a tetrahedral geometry.

The final Rietveld refinement result of BMFI-HDA (Figure S11 and Table S2) shows that boron-rich T sites are located in T3 and T9 positions (as illustrated in Fig. 4a and S12), respectively. T9 position is also in the four-ring of *mel* CBU (Figure S12a), but T3 locates in the five-rings of *mfi* CBU (Figure S12b). Moreover, one linear HDA lies in Region I and II along the *b*-axis, while another highly distorted (due to its flexibility) located in Region III is observed (Fig. 4a). It is of interest to note that Region III can also be stabilized by inorganic cations Na^+ supporting the 10-ring pore openings along the *a*-axis. For the BMFI-NBA sample, the Rietveld refinement analysis (Figure S13 and Table S2) shows that there is one BA molecule running along the straight channel and another BA molecule stabilizing Region III (Fig. 4b). Furthermore, boron rich positions are also distributed in the four-ring of *mel* CBU and the five-rings of *mfi* CBU (Figure S12). Since there are only 0.24Na^+ within one unit cell, it indicates that most of negative charges from the framework are balanced by the protonated OSDAs, rather than inorganic cations. It is challenging to determine the locations of Na cations accurately through Rietveld refinement. The similar scenario was also observed in the **MFI**-borosilicate templated by ethylenediamines (En) in the previous report

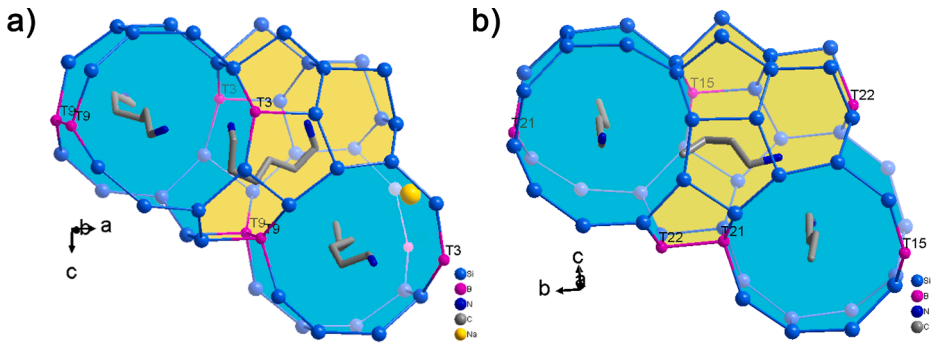

Fig. 4. (a) The locations of HDA, Na^+ and boron-rich positions in the BMFI-HDA. (b) The locations of NBA and boron-rich positions in the BMFI-NBA.

[23].

In this work, firstly, the preferred location of boron atoms, the locations and orientations of OSDAs in **MFI**-type borosilicates templated by TPA^+ have been systemically investigated through Rietveld refinement and simulated annealing against PXRD data. Secondly, based on understanding the structural roles of TPA^+, we successfully replaced TPA^+ by linear organic molecules and inorganic cation Na^+. Another two well-crystallized **MFI**-type borosilicates without any impurity, satisfying with the requirement of the sample quality for Rietveld refinement, were obtained. All the final Rietveld refinements shows that boron atoms preferred locating in four- or five-rings for BMFI samples. This insightful structural information will shed light on 1) distributions of Bronsted acids (B—OH—Si) and 2) the following precise post-synthesis of these well-characterized **MFI**-type borosilicates.

CRediT authorship contribution statement

Xiaona Liu: Formal analysis, Investigation. **Nana Yan:** Investigation. **Chao Ma:** Investigation. **Lei Wang:** Investigation. **Peng Tian:** Supervision. **Peng Guo:** Conceptualization, Project administration, Supervision. **Zhongmin Liu:** Supervision.

Declaration of Competing Interest

The authors declare that they have no known competing financial interests or personal relationships that could have appeared to influence the work reported in this paper.

Acknowledgements

This work was supported by the National Natural Science Foundation of China (21972136, 21991090, 21606221, 21991091), Key Research Program of Frontier Sciences, CAS (QYZDB-SSW-JSC040), the Pioneer Hundred Talents Program, CAS (Y706071202), the Dalian National Laboratory for Clean Energy Cooperation Fund, CAS (DNL201908), and Scholarship from STOE.

Appendix A. Supplementary material

Supplementary data to this article can be found online at https://doi.org/10.1016/j.inoche.2021.108467.

References

[1] Database of Zeolite Structures, Database of Zeolite Structures. (http://www.iza-structure.org/databases/). http://www.iza-structure.org/databases/ (accessed December 19, 2020).
[2] P. Guo, N. Yan, L. Wang, X. Zou, Database Mining of Zeolite Structures, Cryst. Growth Des. 17 (2017) 6821–6835, https://doi.org/10.1021/acs.cgd.7b01410.
[3] J. RSseler, G. Heitmann, W.F. HSlderich, Vapour-phase Beckmann rearrangement using B-MFI zeolites, in: Appl. Catal. A, General, SEOUL, SOUTH KOREA, 1996: pp. 319–333.
[4] P. Guo, K. Strohmaier, H. Vroman, M. Afeworki, P.I. Ravikovitch, C.S. Paur, J. Sun, A. Burton, X. Zou, Accurate structure determination of a borosilicate zeolite EMM-26 with two-dimensional 10 × 10 ring channels using rotation electron diffraction, Inorg. Chem. Front. 3 (2016) 1444–1448, https://doi.org/10.1039/C6QI00262E.
[5] D. Xie, L.B. McCusker, C. Baerlocher, L. Gibson, A.W. Burton, S.-J. Hwang, Optimized Synthesis and Structural Characterization of the Borosilicate MCM-70, J. Phys. Chem. C. 113 (2009) 9845–9850, https://doi.org/10.1021/jp903500q.
[6] S. Smeets, L.B. McCusker, C. Baerlocher, D. Xie, C.-Y. Chen, S.I. Zones, SSZ-87: A Borosilicate Zeolite with Unusually Flexible 10-Ring Pore Openings, J. Am. Chem. Soc. 137 (2015) 2015–2020, https://doi.org/10.1021/ja512411b.
[7] D. Xie, L.B. McCusker, C. Baerlocher, Structure of the Borosilicate Zeolite Catalyst SSZ-82 Solved Using 2D-XPD Charge Flipping, J. Am. Chem. Soc. 133 (2011) 20604–20610, https://doi.org/10.1021/ja209220a.
[8] A.B. Pinar, L. Gómez-Hortigüela, L.B. McCusker, J. Pérez-Pariente, Controlling the Aluminum Distribution in the Zeolite Ferrierite via the Organic Structure Directing Agent, Chem. Mater. 25 (2013) 3654–3661, https://doi.org/10.1021/cm4018024.
[9] T. Yokoi, H. Mochizuki, S. Namba, J.N. Kondo, T. Tatsumi, Control of the Al Distribution in the Framework of ZSM-5 Zeolite and Its Evaluation by Solid-State NMR Technique and Catalytic Properties, J. Phys. Chem. C. 119 (2015) 15303–15315, https://doi.org/10.1021/acs.jpcc.5b03289.
[10] M. Liu, T. Yokoi, M. Yoshioka, H. Imai, J.N. Kondo, T. Tatsumi, Differences in Al distribution and acidic properties between RTH-type zeolites synthesized with OSDAs and without OSDAs, Phys. Chem. Chem. Phys. 16 (2014) 4155, https://doi.org/10.1039/c3cp54297a.
[11] C.-Y. Chen, S.I. Zones, Post-Synthetic Treatment and Modification of Zeolites, in: J. Čejka, A. Corma, S. Zones (Eds.), Zeolites: Synthesis, Catalysis and Applications, Wiley-VCH Verlag GmbH & Co., KGaA, Weinheim, Germany, 2010, pp. 155–170, 10.1002/9783527630295.ch6.
[12] S.I. Zones, A. Benin, S.-J. Hwang, D. Xie, S. Elomari, M.-F. Hsieh, Studies of Aluminum Reinsertion into Borosilicate Zeolites with Intersecting Channels of 10- and 12-Ring Channel Systems, J. Am. Chem. Soc. 136 (2014) 1462–1471, https://doi.org/10.1021/ja4100194.
[13] J.C. Jansen, Ruiter R. De, E. Biron, H. van Bekkum, Isomorphous substitution of Si in zeolite single crystals. Part II. On the boron distribution and coordination in [B]-ZSM-5, Stud. Surf. Sci. Catal. 49 (1989) 679–688.
[14] H. Kessler, J.M. Chezeau, J.L. Guth, H. Strub, G. Coudurier, N.m.r. and i.r. study of B and B-AI substitution in zeolites of the MFI-structure type obtained in non-alkaline fluoride medium, Zeolites. 7 (1987) 360–366.
[15] J. Bae, J. Cho, J.H. Lee, S.M. Seo, S.B. Hong, EU-12: A Small-Pore, High-Silica Zeolite Containing Sinusoidal Eight-Ring Channels, Angew. Chem. Int. Ed. 55 (2016) 7369–7373, https://doi.org/10.1002/anie.201600146.
[16] M. Dodin, J.-L. Paillaud, Y. Lorgouilloux, P. Caullet, E. Elkaïm, N. Bats, A Zeolitic Material with a Three-Dimensional Pore System Formed by Straight 12- and 10-Ring Channels Synthesized with an Imidazolium Derivative as Structure-Directing Agent, J. Am. Chem. Soc. 132 (2010) 10221–10223, https://doi.org/10.1021/ja103648k.
[17] R. Simancas, J.L. Jordá, F. Rey, A. Corma, A. Cantín, I. Peral, C. Popescu, A New Microporous Zeolitic Silicoborate (ITQ-52) with Interconnected Small and Medium Pores, J. Am. Chem. Soc. 136 (2014) 3342–3345, https://doi.org/10.1021/ja411915c.
[18] D.E. Akporiaye, H. Fjellvag, UiO-6: a novel 12-ring A1PO4, made in an inorganic-organic cation system, Chem. Commun. 1553–1554 (1996).
[19] B.J. Campbell, A.K. Cheetham, G. Bellussi, L. Carluccio, G. Perego, R. Millini, D. E. Cox, The synthesis of the new zeolite, ERS-7, and the determination of its structure by simulated annealing and synchrotron X-ray powder diffraction, Chem. Commun. (1998) 1725–1726, https://doi.org/10.1039/a803572e.
[20] N. Yan, H. Xu, W. Zhang, T. Sun, P. Guo, P. Tian, Z. Liu, Probing locations of organic structure-directing agents (OSDAs) and host-guest interactions in CHA -type SAPO-34/44, Microporous and Mesoporous Mater. 264 (2018) 55–59, https://doi.org/10.1016/j.micromeso.2018.01.002.
[21] L. Wang, H. Xu, N. Yan, S. Correll, S. Xu, P. Guo, P. Tian, Z. Liu, Exploring Brønsted acids confined in the 10-ring channels of the zeolite ferrierite, CrystEngComm. 20 (2018) 699–702, https://doi.org/10.1039/C7CE01967J.
[22] S. Smeets, L.B. McCusker, C. Baerlocher, S. Elomari, D. Xie, S.I. Zones, Locating Organic Guests in Inorganic Host Materials from X-ray Powder Diffraction Data, J. Am. Chem. Soc. 138 (2016) 7099–7106, https://doi.org/10.1021/jacs.6b02953.
[23] L. Leardini, A. Martucci, G. Cruciani, The unusual thermal behaviour of boron-ZSM-5 probed by “in situ” time-resolved synchrotron powder diffraction, Microporous and Mesoporous Mater. 173 (2013) 6–14, https://doi.org/10.1016/j.micromeso.2013.01.036.